PCCP

ROYAL SOCIETY OF CHEMISTRY

PAPER

Cite this: *Phys. Chem. Chem. Phys.*, 2020, **22**, 11053

Salt parameterization can drastically affect the results from classical atomistic simulations of water desalination by MoS_2 nanopores†

João P. K. Abal, [a] José Rafael Bordin *[b] and Marcia C. Barbosa[a]

Received 28th January 2020,
Accepted 20th April 2020

DOI: 10.1039/d0cp00484g

rsc.li/pccp

Water scarcity is a reality in our world, and scenarios predicted by leading scientists in this area indicate that it will worsen in the next decades. However, new technologies based on low-cost seawater desalination can prevent the worst scenarios, providing fresh water for humanity. With this goal, membranes based on nanoporous materials have been suggested in recent years. One of the materials suggested is MoS_2, and classical Molecular Dynamics (MD) simulation is one of the most powerful tools to explore these nanomaterials. However, distinct force fields employed in MD simulations are parameterized based on distinct experimental quantities. In this paper, we compare two models of salt that were built based on distinct properties of water–salt mixtures. One model fits the hydration free energy and lattice properties, and the second fits the crystal density and the density and the dielectric constant of water and salt mixtures. To compare the models, MD simulations for salty water flow through nanopores of two sizes were used – one pore big enough to accommodate hydrated ions, and one smaller in which the ion has to dehydrate to enter – and two rigid water models from the TIP4P family – TIP4P/2005 and TIP4P/ε. Our results indicate that the water permeability and salt rejection by the membrane are more influenced by the salt model than by the water model, especially for the narrow pore. In fact, completely distinct mechanisms were observed, and they are related to the characteristics employed in the ion model parameterization. The results show that not only can the water model influence the outcomes, but the ion model plays a crucial role when the pore is small enough.

1 Introduction

One of the greatest challenges of our time is concerned with water scarcity. Currently, our freshwater resources are dwindling at an unprecedented rate due to a high imbalance between clean water demand and total supply.[1] In the face of growing water scarcity, it is critical to understand the potential of salty water desalination as a long-term water supply option.[2] The Reverse Osmosis (RO) system is considered the leading desalination process and the best available option in terms of energy consumption.[3] This technique is based on a membrane separation method. However, the energy and monetary cost of RO with the current membranes are high mainly because of membrane fouling phenomena. A new and promising technology is to use membranes made of materials[4] such as graphene[5,6] and molybdenum disulfide,[7] which show improved permeability potential and exceptional separation capability.

The key component of a good membrane is the balance between water permeability and salt rejection, in such a way that the next-generation membranes need to be very selective.[8] Molecular dynamics simulations are a powerful tool to mimic a reverse osmosis system at the nanoscale.[9] It helps us to get insights to design new membrane materials and better understand the water–salt–nanopore relationship.[6] The water flux through the membrane can be generally related to its specific permeability by the following expression: $A_m = \phi/(P - \Pi)$, in which A_m is the membrane specific permeability, ϕ is the water flux, P is the applied pressure and Π is the osmotic pressure. All these quantities can be obtained or controlled by designing the system for molecular dynamics simulations.

Graphene based nanomembranes are well known in the literature[5,10] and have been extensively studied, showing efficiency in water desalination.[4,11] Another promising material is nanoporous molybdenum disulfide (MoS_2). Its efficiency has been investigated by molecular dynamics simulations[12–15] and experimental work,[16–19] showing that the combination of hydrophobic and hydrophilic sites in the nanopore can increase the desalination performance.

[a] *Institute of Physics, Federal University of Rio Grande do Sul, 91501-970, Porto Alegre, Brazil. E-mail: joao.abal@ufrgs.br, marcia.barbosa@ufrgs.br*
[b] *Department of Physics, Institute of Physics and Mathematics, Federal University of Pelotas, Rua dos Ipês, Capão do Leão, RS, 96050-500, Brazil. E-mail: jrbordin@ufpel.edu.br*

† Electronic supplementary information (ESI) available. See DOI: 10.1039/d0cp00484g

Molecular dynamics simulations are a suitable theoretical approach to understand the physics behind nanofluidic systems as they allow for probing the microscopic behavior of atoms while performing timescale feasible simulations.[20] In addition, to represent the system computationally one has to face the challenge of designing a model capable of encoding the main physics of the problem. It is said that the model chosen to represent the interactions of the atoms is the seed from which the whole dynamics arise following the classical equations of motion. In the specific case of classical atomistic molecular dynamics simulations, most of the force fields use simple additive, nonpolarizable, and pairwise potentials for atomic interactions.[21–26] In the case of water, rigid nonpolarizable models are extensively employed in simulations of bulk[27] and nanoconfined[28–32] systems. Efforts have been made to include polarization in classical simulations,[33–36] but nonpolarizable salt and water remain as the main models in MD simulations of desalination.

Another issue that has to be handled with care relies on the optimization of specific ion parameters for specific water models. As Döpke and co-authors have recently shown,[37] salt models optimized for SPC/E and TIP3P water can lead to wrong predictions when dissolved in TIP4P/2005 water. This is relevant as the TIP4P/2005[38] model is one of the best and most employed rigid water models.

In recent work about water desalination by nanopores[7,14,39–43] the ion model proposed by Joung and Cheatham[44] has been employed. This model, which will be referred to as NaCl/*J*, was parameterized based on the hydration free energies of the solvated ions and lattice parameters of salt crystals and has good agreement with several experimental studies. These parameters were optimized in combination with some of the most classical water models, as SPC/E, TIP3P, or TIP4P/Ew water. Also, as Liu and Patey[42] and Döpke *et al.*[37] discuss in their work, the ion parameters optimized for TIP4P/Ew can be transferred to TIP4P/2005 water without a loss of accuracy. On the other hand, the dielectric discontinuity of water near interfaces and nanopores plays a crucial role in salt behavior.[45–47] Recently, Fuentes and Barbosa proposed the NaCl/ε model.[48] This model was parameterized to reproduce the experimental values of the density of the crystal and the density and dielectric constant of the mixture of salt with water in a diluted solution when combined with the TIP4P/ε rigid water model. To reproduce these properties and correct for the nonpolarizability of the model they propose a screening factor in the Coulomb interaction – usually, nonpolarizable models are parametrized based on the Lennard-Jones (LJ) potential parameters only.

Besides that, the atomic partial charge of MoS_2 atoms leads to exotic flux behaviors. The molybdenum in the centre attracts water, and then the sulfur on the other side pushes it away.[7,49,50] The charge distribution affects the overall flux as reported by previous studies.[51–53] A preliminary simulation is documented in the ESI† for further information on this topic.

In this paper, we answer the question about how distinct ionic models influence the study of MoS_2 membrane water desalination. To do so we compare a model of ions constructed based on hydration and crystal properties, and a model constructed to reproduce the density and dielectric constant of water and salt mixtures. To compare the models, two nanopore sizes were used: one pore big enough to accommodate hydrated ions, and one smaller in which the ion has to dehydrate to enter. Our paper is organized as follows. In Section 2 we introduce our model and the details about the simulation method. In Section 3 we show and discuss our results, and the conclusions are presented in Section 4.

2 Methods and simulational details

One of the most employed methodologies to simulate the saltwater desalination process in MD simulations[12–15] is based on the creation of a box with the membrane located between two confined reservoirs, one of pure water and another one with saltwater, as we show in Fig. 1. The reservoirs can be confined by graphene barriers, for example. This barriers are used as pistons to control the confined solution pressure. To mimic the water driving force throughout the membrane, one has to apply different pressures in each reservoir. These pressures are simulated by applying a force F on each piston atom as calculated by $F = (\Delta P \cdot A)/n$, where P is the desired pressure, A refers to the area that the pressure is applied on (equal to the piston surface area), and n is the number of carbon atoms in each carbon sheet.

Molecular dynamics was performed using the LAMMPS package.[55] The initial system in between the graphene barriers is $4 \times 4 \times 12.5$ nm in the x, y, and z directions, respectively. Periodic boundary conditions were used in all directions. By doing that, one has to use a simulation box large enough in the z direction in order to guarantee that the molecules don't interact with each other across that boundary. The saltwater used has an almost 1 mol L^{-1} solute concentration (170 ions for 4930 water molecules), higher than the average seawater salinity of 0.6 mol L^{-1}. The pure water side contains 1550 molecules.

The salt and water Lennard-Jones parameters and charges were taken from the papers that proposed each model: the NaCl/ε model,[48] the NaCl/J[44] model, the Tip4p/ε[56] model and Tip4p/2005.[38] The parametrization of a reactive many-body

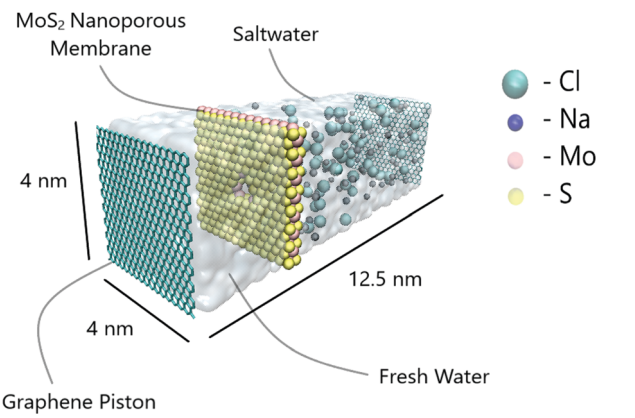

Fig. 1 The illustration of a typical desalination box of $4 \times 4 \times 12.5$ nm confined by graphene barriers. The fresh water reservoir and saltwater reservoir are separated by a MoS_2 membrane and are connected by the designed nanopore. Image created using the VMD software.[54]

Table 1 The Lennard-Jones parameters and atomic charges employed in the simulations

	σ_{LJ} [Å]	ε_{LJ} [kcal mol^{-1}]	Charge (e)
Na-ε[48]	2.52	0.0346	1.0
Cl-ε[48]	3.85	0.3824	−1.0
Na-J[44]	2.18	0.1684	1.0
Cl-J[44]	4.92	0.0117	−1.0
O-Tip4p/ε[56]	3.165	0.1848	−1.054
H-Tip4p/ε[56]	0.0	0.0	0.5270
O-Tip4p/2005[38]	3.1589	0.1852	−1.1128
H-Tip4p/2005[38]	0.0	0.0	0.5564
Mo[57]	4.20	0.0135	0.6
S[57]	3.13	0.4612	−0.3
C[57]	3.40	0.0860	0.0

potential was used as LJ parameters and charges values for molybdenum and sulfur, as proposed by Kadantsev and Hawrylak.[57] The carbon parameters from the graphene piston were taken from the seminal work on confined water by Hummer and co-workers.[58] The models employed in this work are summarized in Table 1. For simplicity, the MoS_2 membrane remained fixed in all simulations, and the graphene sheet has freedom only in the flow direction. For the non-bonded interactions, the Lorentz–Berthelot mixing rules were employed. The long-range electrostatic interactions were calculated by the particle–particle–particle–mesh method and the LJ cutoff distance was 1 nm. The SHAKE algorithm was used to keep the water molecules rigid.

First, each energy simulation was minimized for 0.5 ns in the *NVE* ensemble. It means that the graphene sheets are frozen at that time. After that, the simulations were equilibrated with the constant number of particles, pressure, and temperature (*NPT*) ensemble for 1 ns at 1 bar and 300 K, as illustrated in Fig. 2-up. Pressure control was performed by leaving the graphene pistons free to move in the z-direction and applying a force on each carbon atom in order to produce the desired ambient pressure. After some simulation steps, the solution equilibrates and the piston pressure reaches the equilibrium density at 1 g cm^{-3}. Then, the graphene sheets were frozen and 2 ns simulations in the *NVT* ensemble were performed to further equilibrate the system. The Nosé–Hoover thermostat was used with a time constant of 0.1 ps.[59,60]

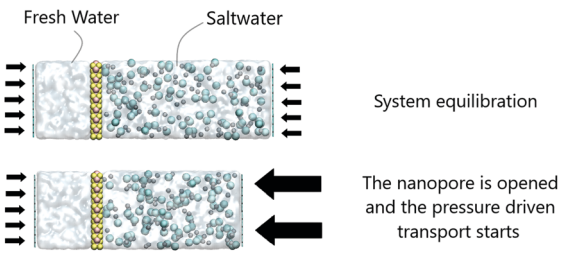

Fig. 2 The illustration of the system equilibration with the nanopore closed (top) and the schematic depiction of the non-equilibrium scheme when the nanopore is opened (bottom): the pressure on the left graphene sheet is constant and equal to atmospheric pressure, 1 bar, while distinct higher values are applied on the right graphene sheet, ranging from 1000 to 10 000 bar.

Next, the nanopore was opened by removing the desired atoms of molybdenum and sulfur in order to keep the membrane charge neutral. The two nanopores studied have 0.74 nm and 0.97 nm diameters respectively. The nanopore sizes were calculated by using the center-to-center distance of atoms. Finally, external pressure was applied on the feed side and non-equilibrium running was carried out for 10 ns, as illustrated in Fig. 2-bottom. Each run was averaged over 3 sets of simulations with different initial thermal velocity distributions. The feed pressures range from 1000, 2500, and 5000 to 10 000 bar. We used such high pressures for statistical purposes.

3 Results and discussion

Distinct models can lead to different water flow rates in nanopores because the different number of sites, flexibility, partial charges, and LJ parameters can strongly change the observed flow.[28] In a similar way, the ion parameters can affect the ionic blockage and binding in biological[21,61] and synthetic nanopores.[62–65] In fact, a considerable number of factors affect the ion entry in nanopores.[62,66] In order to investigate the role of screening, we evaluate the water and ion flow through nanopores with diameters of 0.97 nm or 0.74 nm using two distinct water and ion models. For the wider diameter, the ion enters in the nanopore screened by water, while for the smaller diameter the ion has to strip out the water in order to penetrate the pore. These two cases allow us to compare not only the model effect but the screening effect. For the sake of comparison, the results with the NaCl/J model and smallest nanopore are compared to the results presented in ref. 7 and documented in the ESI.†

Despite the fact that TIP4P/2005 and TIP4P/ε both have 4 charged sites, we can expect that the distinct values of their parameters can affect the permabillity of pure water through nanopores. However, as Losey and co-workers have shown in recent work,[28] the TIP4P and TIP4P/2005 water models have similar flow rates. In agreement with this result, our simulations show that when the same model of salt is employed, the membrane permeability for both TIP4P/2005 and TIP4P/ε is approximately the same – the differences are smaller than the error bar, as we can see in Fig. 3, from both nanopore sizes. Changing the salt model to NaCl/ε affects the water permeation in the widest nanopore at the higher values of pressure. As we can see in Fig. 3(a), when the applied pressure is 10 000 bar the combination of TIP4P/ε + NaCl/ε shows a higher water flow rate. On the other hand, the water permeability is small for this combination in the case of nanopores with a 0.74 nm diameter, as shown in Fig. 3(b). Actually, the permeability is small and approximately constant for the three smallest values of the applied pressure – a huge pressure gradient is necessary to create a bigger water flow through the nanopore, a water flow capable of pushing the blocking ion through the nanopore.

The distinct values of water permeation for each combination of water and salt models, as well as for each nanopore size, Fig. 3, are related to distinct salt rejection. As we show in Fig. 4(a), the salt rejection in the wider pore decreases with the applied

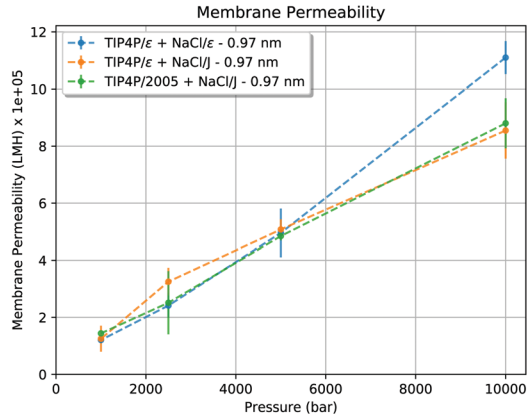

(a)

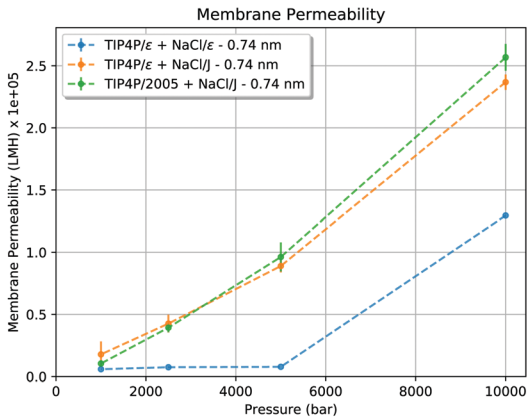

(b)

Fig. 3 Membrane water permeability for distinct combinations of water and salt models and (a) nanopores with a 0.97 nm diameter and (b) with a 0.74 nm diameter. Error bars are the deviation from the mean value – error bars smaller than the point are not shown.

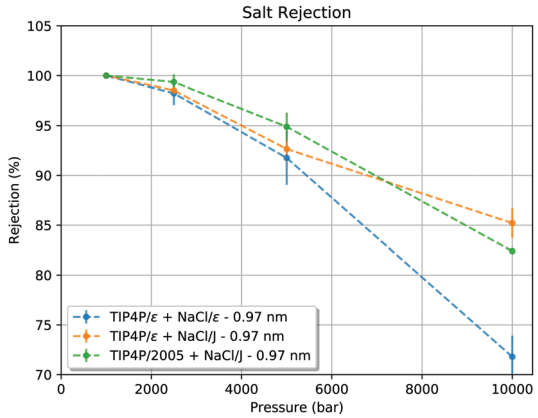

(a)

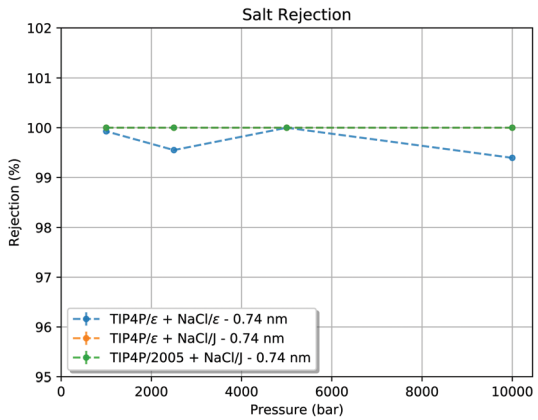

(b)

Fig. 4 Salt rejection for distinct combinations of water and salt models and (a) nanopores with a 0.97 nm diameter and (b) with a 0.74 nm diameter. Error bars are the deviation from the mean value – error bars smaller than the point are not shown.

pressure, and NaCl/ε has the smallest rejection at higher pressure – in agreement with the higher water permeability. For the narrow pore, the system with NaCl/*J* salt shows 100% rejection as shown in Fig. 4(b) and in agreement with our previous results.[13] In the case of the Na/ε salt model, a few ions can cross the pore. The membrane specific permeability, computed from the slope of Fig. 3, was obtained for each mixture and nanopore size and the results are summarized in Table 2.

To understand the water and ion permeation through the pore, we evaluate the Mean Passage Time (MPT) of the different ion models through the nanopore with the two studied diameters. As we show in Fig. 5(a) and (b), the Cl/ε anions are responsible for the nanopore blockage when this model is employed. Despite the case of 10 000 bar applied pressure, in all cases the chlorine takes a long time to pass the pore and therefore is the ion blocking the pore. Even for the wider nanopore, the blockage time is relevant at lower pressures, with the Cl anion remaining for almost 5 ns, or half of the production time, inside the pore. On the other hand, the Cl/*J* anion remains for short times inside the nanopore with a 0.97 nm diameter, which explains the higher water permeability and smaller ionic rejection, and never enters the smallest pore, as shown in Fig. 5(b).

Table 2 The membrane specific permeabilities (A_m) obtained for such nanopore sizes considering a nanopore density of 6.25×10^{12} cm^{-2}. The numbers inside the parentheses are the membrane specific permeability standard deviations evaluated in this work

Mixture	A_m [LMH/bar]	Diameter [nm]
TIP4P/ε–NaCl/ε	108.2 (17.5)	0.97
TIP4P/ε–NaCl/*J*	104.1 (28.6)	0.97
TIP4P/2005–NaCl/*J*	118.7 (25.8)	0.97
TIP4P/ε–NaCl/ε	5.9 (5.1)	0.74
TIP4P/ε–NaCl/*J*	17.2 (5.7)	0.74
TIP4P/2005–NaCl/*J*	18.4 (5.8)	0.74
Nanopore density		6.25×10^{12} cm^{-2}

For the smaller pore, the fact that distinct mechanisms are responsible for the ionic rejection is interesting. For NaCl/ε the pore is blocked by the chlorine anion (see Fig. 5(b) and 8), while for the NaCl/*J* model the chlorine never enters the pore. In addition, the sodium cation takes a short time to pass the wider nanopore, as illustrated in Fig. 5(c). At this point, it is relevant

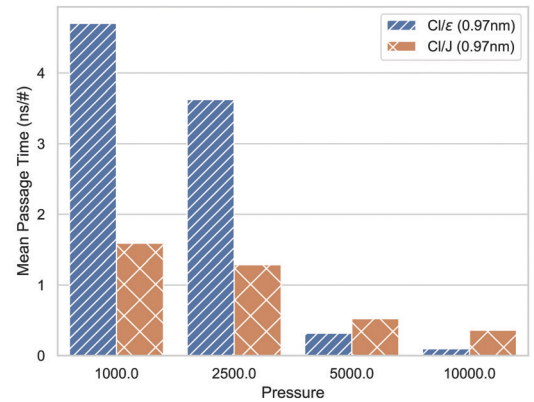

(a)

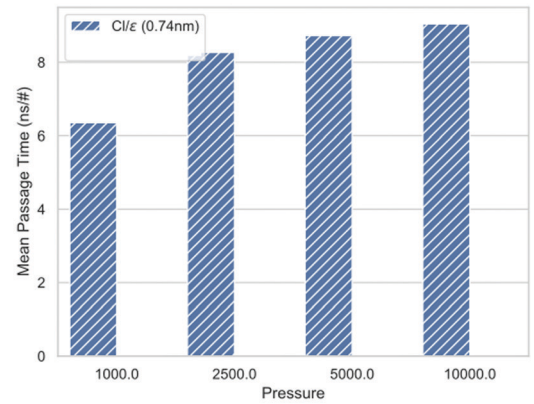

(b)

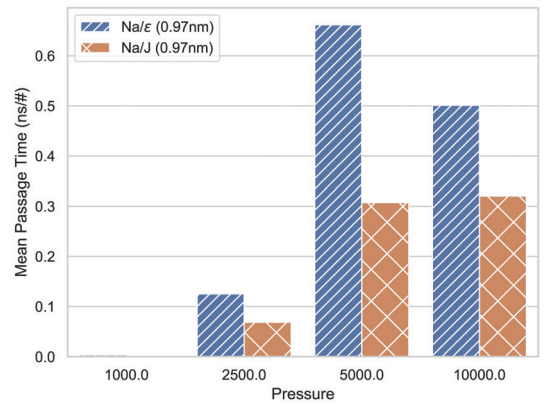

(c)

Fig. 5 Mean passage time (MPT) *versus* applied pressure for different models and nanopore diameters. (a) The Cl/ε and Cl/*J* MPT in the 0.97 nm diameter are compared. Although the anions remain for a considerable amount of time inside the nanopore, water still can flow as shown in Fig. 8. (b) The Cl/ε MPT in the 0.74 nm diameter is shown. Cl/ε remains for almost the total simulation time blocking the nanopore. In contrast, Cl/*J* don't enter in the nanopore and therefore it is not shown. (c) The Na/ε and Na/*J* MPT in the 0.97 nm diameter are compared. The Na/ε and Na/*J* cases for the 0.74 nm diameter are not shown because they never enter in that nanopore.

to emphasize that the ionic passage through small pores has two main events:[47] first the ion must hit the pore, and secondly it needs to have enough energy to overcome the energetic penalty related to leaving the bulk, entering the pore with a distinct dielectric constant, and crossing the pore to the bulk again. The first process is a classical problem from statistical mechanics, depending mainly on the system density and pore area.[67,68] In the second process the penalties can depend on the nanopore size, ion hydration, ion charge, pore chemical characteristics and pore geometry.[47,62] Therefore, we will now analyze how the salt model properties influence the ion translocation event.

The ion translocation process is analyzed by the Potential of Mean Force (PMF), which quantifies the energy profile as the ion leaves the bulk, enters the pore, crosses it and leaves to the other bulk region. Here, the PMF calculations were performed by preparing a set of different systems in which one specific ion is frozen in a position along the z direction, aligned with the center of the nanopore. At this specific position, we run 0.5 ns of simulation, the time required for the salt and water around the ion to achieve equilibrium, with the pore closed and without a pressure gradient. Then, the external pressure is increased to 1000 bar and the nanopore is opened. With the ion still fixed in space, we evaluated the force felt by this ion for another 0.5 ns. After that, we increased the z position of the ion by δz = 0.5 Å, and repeated the steps in the equilibrium and in the non-equilibrium and so on until the ion crosses the pore to the other bulk region. After that, the PMF was obtained by the integration of the total mean force along the z direction. In this procedure the ions are forced to assume a position along the central pore axis independent of ion hydration. Therefore, this PMF doesn't take into account the dehydration energy penalty – the dehydration will be discussed further.

The PMF calculations were done using only the TIP4P/ε water for two complementary reasons. First, the permeation seems to be more sensitive to the ion model rather than to the water model. Second, the electrostatic barrier related to the dielectric discontinuity from the bulk water to the nanopore region is relevant, and this water model was parameterized to provide the correct value of the bulk water dielectric constant.[56] In the same spirit, NaCl/ε was parameterized to reproduce the dielectric constant of the mixture of salt with water in a diluted solution.[48]

As we show in Fig. 6(a), the energetic penalty for a sodium ion to leave the bulk and to enter the nanopore with diameter 0.74 nm is more than 5 times the thermal energy at 300 K, $k_BT \approx 0.6$ kcal mol^{-1}. This explains why we have to apply a huge pressure to observe a Na cation inside this small pore. On the other hand, the energy barrier for a Cl anion is much smaller, comparable with the thermal energy, for both models. Therefore the anion can penetrate the pore only due to thermal fluctuations at room temperature. However, the central well has a deepness of 4 to 5 times k_BT, created by the attraction with the central layer of positively charged molybdenum. Then the Cl^- gets trapped. This, however, does not explain why Cl/ε enters and blocks the nanopore, while Cl/*J* never leaves the bulk to the pore.

The reason for the distinct blockage when the two models are compared for the nanopore with diameter 0.74 nm is that the NaCl/*J* model is more hydrated than the NaCl/ε model.

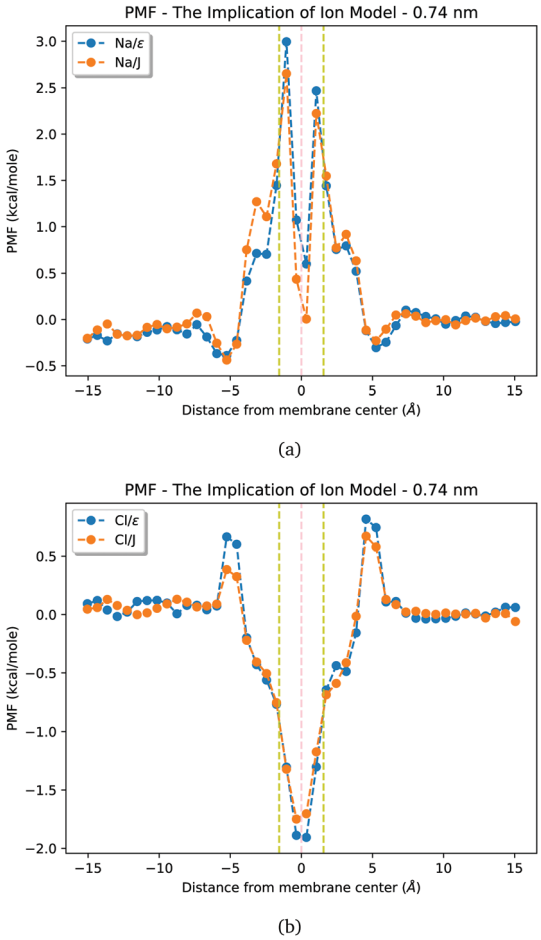

Fig. 6 PMF inside nanopores with a 0.74 nm diameter for (a) sodium and (b) chlorine ions. The central vertical pink dashed line represents the molybdenum layer position, and the vertical yellow dashed lines around it the sulfur layer position.

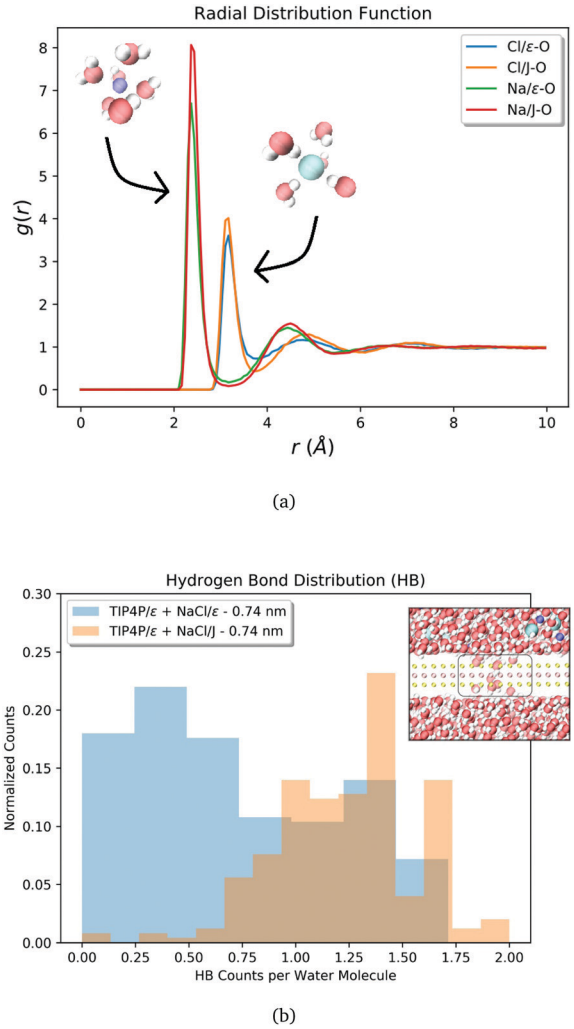

Fig. 7 (a) Bulk ion–oxygen radial distribution at 300 K and 1000 bar. (b) Hydrogen bond (HB) distribution near the pore. In the inset we show the region considered to evaluate the distribution.

The different screening factors employed affect the water distribution around the ions. In Fig. 7(a) we show the radial distribution function, $g(r)$, of the oxygen atoms of the water molecules around the distinct species of ions. For the sodium ions, the peaks are smaller for the Na/ε than for the Na/J model. For the Na ion, however, the peak distances are the same and the water structure around Na is independent of the water model. On the other hand, for the chlorine ions, not only are the peaks for Cl/ε smaller, but the water seems more disordered: the depletion between the first and second hydration layer is shallower, and the curve is almost flat after this second peak. This is confirmed when we evaluate the hydrogen bond (HB) distribution near the pore, as shown in Fig. 7(b) (the HB distribution was obtained by following distance and angular criteria considering $r_{O\text{–}O} < 3.5$ Å and $\theta_{OH\text{–}O} < 30^{\circ}$).[69] As we can see, for the NaCl/ε model more then 60% of the water molecules form less than one HB on average. On the other hand, when the NaCl/J model is employed each water molecule forms more than one hydrogen bond. Therefore the salt model not only affects the ion wettability, but can also effectively change the water HB network. Then, due the higher hydration and the higher

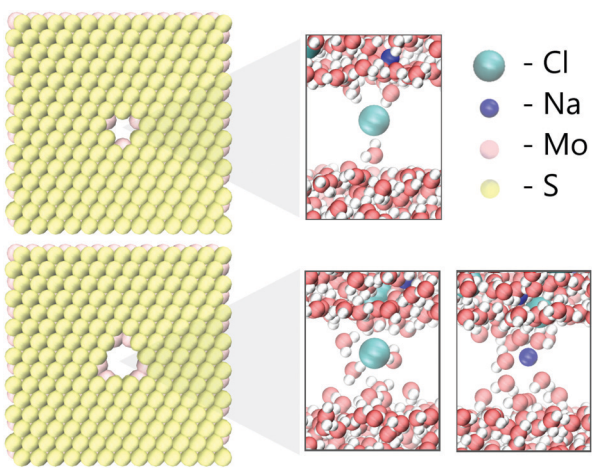

Fig. 8 Snapshots of the simulation showing that for the smaller nanopore (upper snapshot) only dehydrated Cl/ε ions can penetrate the pore, while for the nanopores with diameter 0.97 nm we observe permeation of both hydrated ionic species and models.

number of HBs by water molecules, the Cl/ε can strip out this water easily in comparison to the Cl/J model and enter the channel. This "water stripping" is essential, since the small nanopore diameter of 0.74 nm makes it impossible for a hydrated ion to penetrate the pore – as we have observed and show in the upper snapshot of Fig. 8.

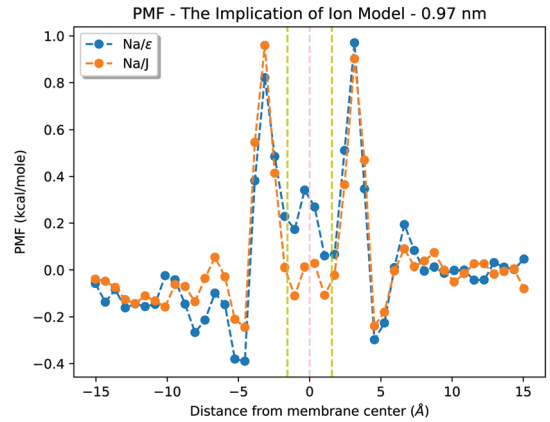

(a)

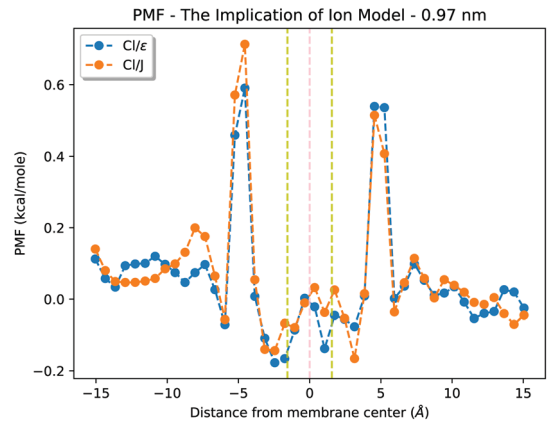

(b)

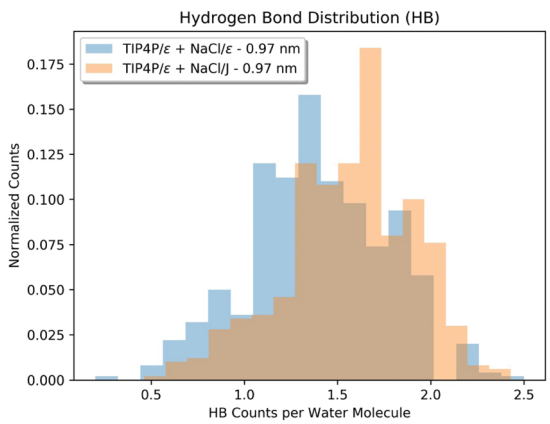

(c)

Fig. 9 PMF inside nanopores with a 0.97 nm diameter for (a) sodium and (b) chlorine ions. The central vertical pink dashed line represents the molybdenum layer position, and the vertical yellow dashed lines around it the sulfur layer position. (c) Hydrogen bond distribution near the pore.

The nanopore with diameter 0.97 nm is wide enough to accommodate hydrated ions, as we show in the lower panel of Fig. 8. This hydration makes the dielectric discontinuity between the bulk and the pore small, decreasing the energetic penalty for the ion current through the nanopore. The barrier, illustrated in Fig. 9(a), for the sodium ions is now smaller than twice the thermal energy. Therefore, the ions can cross the pore as the pressure increases, as we have observed in Fig. 4(a). Also, the depth of the well for Na/ε is small – so we observe a smaller ion rejection. This is also a consequence of the screening of the Coulomb interaction between the salt and the pore ions, which should rule the PMF when the ions are hydrated and the dielectric discontinuity is small. And, for this nanopore, we do not observe a significant difference in the PMF for both Cl models, which can explain why the mean passage times of the chlorine ions for both models are comparable in the wide pores, especially at high pressure, as shown in Fig. 5(a). In a similar way, the water HB distribution near the pore region is similar for both ion models, as Fig. 9(c) shows. The small difference for NaCl/ε leading to fewer HBs can also be associated with the small ion rejection observed for this salt model.

These results indicate that the effect of ion rejection depends on the ion model applied. In one case, using the model that did not reproduce properly the dielectric constant of water and salt mixtures, the rejection is due to the dielectric discontinuity and the energetic penalty associated with the ion dehydration. In the other case, employing the model that reproduces the bulk dielectric constant of salt and water mixtures, the pore is blocked by the chlorine ion. Obviously, the second case is not interesting since it does not allow water permeation through the pore. This blockage was observed in experiments for single-layer graphene membranes[11] and has also been suggested by DFT modeling of functionalized graphene nanopores.[70] This effect is well known for polymeric membranes[71] and it is a big challenge in reverse osmosis engineering. However, it was not reported experimentally or by simulations for MoS_2 membranes so far we know. These results indicate that extensive research has to be done, especially experimental studies, to see if there is ionic blockage or not for MoS_2 small nanopores as membrane fouling control is one of the most important performance parameters for next-generation membrane materials.[8]

4 Conclusions

We have performed an extensive study on how the selection of the ionic model can affect the water flow and ionic rejection by MoS_2 membranes. We employed two water models from the rigid TIP4P family: the traditional and well-established TIP4P/2005, and TIP4P/ε, recently proposed to provide the correct value of the bulk water dielectric constant. For the salt model we chose the model proposed by Joung,[44] namely NaCl/J, and NaCl/ε.[48] The second salt model, combined with the TIP4P/ε water, can reproduce the dielectric constant of water and salt mixtures.

Our simulations indicate that the water and ion permeation through the nanopores is more sensitive to the ion model than

to the water model employed. In fact, the screening proposed in NaCl/ε leads to the ionic blockage of the nanopore with a small diameter. This mechanism was not observed previously. Also, the water around NaCl/*J* ions is more structured, which influences the ion entrance into the pore.

These results indicate that distinct mechanisms can occur depending on the salt model, not only distinct quantitative results but completely different physical behaviors. Besides that, it is well known that the next generation membrane materials for desalination technology must be very selective and fouling resistant.[72] In order to clarify this point an experimental investigation is necessary on MoS_2 nanopores with a diameter comparable with the ion diameter – so the ion has to be dehydrated to penetrate the pore.

Conflicts of interest

There are no conflicts to declare.

Acknowledgements

This work is financially supported by CNPq. We thank CENAPAD/SP, CESUP/UFRGS and SATOLEP/UFPel for the computer time. JRB thanks the Brazilian agencies CNPq and FAPERGS for the financial support.

References

1 WWAP and UNESCO, The United Nations world water development report 2019: leaving no one behind, United Nations Educational, Scientific and Cultural Organization, 2019.
2 E. Jones, M. Qadir, M. T. van Vliet, V. Smakhtin and S. mu Kang, *Sci. Total Environ*, 2019, **657**, 1343–1356.
3 M. Qasim, M. Badrelzaman, N. N. Darwish, N. A. Darwish and N. Hilal, *Desalination*, 2019, **459**, 59–104.
4 Y. H. Teow and A. W. Mohammad, *Desalination*, 2019, **451**, 2–17.
5 D. Cohen-Tanugi and J. C. Grossman, *Nano Lett.*, 2012, **12**, 3602–3608.
6 D. Cohen-Tanugi and J. C. Grossman, *Desalination*, 2015, **366**, 59–70.
7 M. Heiranian, A. B. Farimani and N. R. Aluru, *Nat. Commun.*, 2015, **6**, 8616.
8 A. Boretti, S. Al-Zubaidy, M. Vaclavikova, M. Al-Abri, S. Castelletto and S. Mikhalovsky, *npj Clean Water*, 2018, **1**, 5.
9 C. Zhu, H. Li and S. Meng, *J. Chem. Phys.*, 2014, **141**, 18C528.
10 A. Aghigh, V. Alizadeh, H. Wong, M. S. Islam, N. Amin and M. Zaman, *Desalination*, 2015, **365**, 389–397.
11 S. P. Surwade, S. N. Smirnov, I. V. Vlassiouk, R. R. Unocic, G. M. Veith, S. Dai and S. M. Mahurin, *Nat. Nanotechnol.*, 2015, **10**, 459–464.
12 W. Li, Y. Yang, J. K. Weber, G. Zhang and R. Zhou, *ACS Nano*, 2016, **10**, 1829–1835.
13 M. H. Köhler, J. R. Bordin and M. C. Barbosa, *J. Chem. Phys.*, 2018, **148**, 222804.
14 M. D. B. Pérez, A. Nicolai, P. Delarue, V. Meunier, M. Drndic and P. Senet, *Appl. Phys. Lett.*, 2019, **114**, 023107.
15 J. Kou, J. Yao, L. Wu, X. Zhou, H. Lu, F. Wu and J. Fan, *Phys. Chem. Chem. Phys.*, 2016, **18**, 22210–22216.
16 H. Li, T.-J. Ko, M. Lee, H.-S. Chung, S. S. Han, K. H. Oh, A. Sadmani, H. Kang and Y. Jung, *Nano Lett.*, 2019, **19**, 5194–5204.
17 Z. Wang, Q. Tu, S. Zheng, J. J. Urban, S. Li and B. Mi, *Nano Lett.*, 2017, **17**, 7289–7298.
18 W. Zhou, X. Zou, S. Najmaei, Z. Liu, Y. Shi, J. Kong, J. Lou, P. M. Ajayan, B. I. Yakobson and J.-C. Idrobo, *Nano Lett.*, 2013, **13**, 2615–2622.
19 W. Hirunpinyopas, E. Prestat, S. D. Worrall, S. J. Haigh, R. A. W. Dryfe and M. A. Bissett, *ACS Nano*, 2017, **11**, 11082–11090.
20 S. Gravelle, https://hal.archives-ouvertes.fr/hal-02375018v1.
21 A. Cordomí, O. Edholm and J. J. Perez, *J. Chem. Theory Comput.*, 2009, **5**, 2125–2134.
22 J. Chandrasekhar, D. C. Spellmeyer and W. L. Jorgensen, *J. Am. Chem. Soc.*, 1984, **106**, 903–910.
23 S. Chowdhuri and A. Chandra, *J. Chem. Phys.*, 2003, **118**, 9719–9725.
24 T. R. Underwood and H. C. Greenwell, *Sci. Rep.*, 2018, **8**, 352.
25 S. Chowdhuri and A. Chandra, *J. Chem. Phys.*, 2001, **115**, 3732–3741.
26 J. L. Aragones, E. Sanz and C. Vega, *J. Chem. Phys.*, 2012, **136**, 244508.
27 I. N. Tsimpanogiannis, O. A. Moultos, L. F. M. Franco, M. B. de M. Spera, M. Erdős and I. G. Economou, *Mol. Simul.*, 2019, **45**, 425–453.
28 J. Losey, S. K. Kannam, B. D. Todd and R. J. Sadus, *J. Chem. Phys.*, 2019, **150**, 194501.
29 M. H. Köhler, J. R. Bordin, C. F. de Matos and M. C. Barbosa, *Chem. Eng. Sci.*, 2019, **203**, 54–67.
30 M. H. Köhler and J. R. Bordin, *J. Phys. Chem. C*, 2018, **122**, 6684–6690.
31 M. H. Köhler, J. R. Bordin, L. B. da Silva and M. C. Barbosa, *Phys. Chem. Chem. Phys.*, 2017, **19**, 12921–12927.
32 M. H. Köhler, J. R. Bordin, L. B. da Silva and M. C. Barbosa, *Phys. A*, 2018, **490**, 331–337.
33 H. Yu, T. W. Whitfield, E. Harder, G. Lamoureux, I. Vorobyov, V. M. Anisimov, A. D. MacKerell and B. Roux, *J. Chem. Theory Comput.*, 2010, **6**, 774–786.
34 Z. Jing, C. Liu, S. Y. Cheng, R. Qi, B. D. Walker, J.-P. Piquemal and P. Ren, *Annu. Rev. Biophys.*, 2019, **48**, 371–394.
35 L. X. Dang, J. E. Rice, J. Caldwell and P. A. Kollman, *J. Am. Chem. Soc.*, 1991, **113**, 2481–2486.
36 J. R. Bordin, R. Podgornik and C. Holm, *Eur. Phys. J.: Spec. Top.*, 2016, **225**, 1693–1705.
37 M. F. Döpke, O. A. Moultos and R. Hartkamp, *J. Chem. Phys.*, 2020, **152**, 024501.
38 J. L. F. Abascal and C. Vega, *J. Chem. Phys.*, 2005, **123**, 234505.
39 M. E. Suk and N. R. Aluru, *J. Chem. Phys.*, 2014, **140**, 084707.

40 D. Cohen-Tanugi, L.-C. Lin and J. C. Grossman, *Nano Lett.*, 2016, **16**, 1027–1033.
41 P. Sahu and S. M. Ali, *Phys. Chem. Chem. Phys.*, 2019, **21**, 21389–21406.
42 L. Liu and G. N. Patey, *J. Chem. Phys.*, 2017, **146**, 074502.
43 G. Lanaro and G. N. Patey, *J. Phys. Chem. B*, 2015, **119**, 4275–4283.
44 I. S. Joung and T. E. Cheatham, *J. Phys. Chem. B*, 2008, **112**, 9020–9041.
45 S. Senapati and A. Chandra, *J. Phys. Chem. B*, 2001, **105**, 5106–5109.
46 Y. Levin, *Rep. Prog. Phys.*, 2002, **65**, 1577–1632.
47 J. R. Bordin, A. Diehl, M. C. Barbosa and Y. Levin, *Phys. Rev. E: Stat., Nonlinear, Soft Matter Phys.*, 2012, **85**, 031914.
48 R. Fuentes-Azcatl and M. C. Barbosa, *J. Phys. Chem. B*, 2016, **120**, 2460–2470.
49 J. Feng, M. Graf, K. Liu, D. Ovchinnikov, D. Dumcenco, M. Heiranian, V. Nandigana, N. R. Aluru, A. Kis and A. Radenovic, *Nature*, 2016, **536**, 197–200.
50 Z. Wang and B. Mi, *Environ. Sci. Technol.*, 2017, **51**, 8229–8244.
51 M. Yang, X. Yang, Q. Wang, K. Wang, X. Fan, W. Liu, X. Liu, J. Liu and J. Huang, *RSC Adv.*, 2014, **4**, 26729–26737.
52 L. Hao, J. Su and H. Guo, *J. Phys. Chem. B*, 2013, **117**, 7685–7694.
53 Z. Huang, Y. Zhang, T. Hayashida, Z. Ji, Y. He, M. Tsutsui, X. S. Miao and M. Taniguchi, *Appl. Phys. Lett.*, 2017, **111**, 263104.
54 W. Humphrey, A. Dalke and K. Schulten, *J. Mol. Graphics*, 1996, **14**, 33–38.
55 S. Plimpton, *J. Comput. Phys.*, 1995, **117**, 1–19.
56 R. Fuentes-Azcatl and M. C. Barbosa, *Phys. A*, 2016, **444**, 86–94.
57 E. S. Kadantsev and P. Hawrylak, *Solid State Commun.*, 2012, **152**, 909–913.
58 G. Hummer, J. C. Rasaiah and J. P. Noworyta, *Nature*, 2001, **414**, 188–190.
59 S. Nosé, *J. Chem. Phys.*, 1984, **81**, 511–519.
60 W. G. Hoover, *Phys. Rev. A: At., Mol., Opt. Phys.*, 1985, **31**, 1695–1697.
61 F. Ashcroft, *Nature*, 2006, **440**, 440–447.
62 O. Beckstein and M. Sansom, *Phys. Biol.*, 2004, **1**, 42–52.
63 Z. He, J. Zhou, X. Lu and B. Corry, *ACS Nano*, 2013, **7**, 10148–10157.
64 J.-P. Hsu, S.-T. Yang, C.-Y. Lin and S. Tseng, *J. Phys. Chem. C*, 2017, **121**, 4576–4582.
65 J. Abraham, K. Vasu and C. e. a. Williams, *Nat. Nanotechnol.*, 2017, **12**, 546–550.
66 O. Beckstein, P. C. Biggin and M. S. P. Sansom, *J. Phys. Chem. B*, 2001, **105**, 12902–12905.
67 Y. Levin, M. A. Idiart and J. J. Arenzon, *Phys. A*, 2004, **344**, 543–546.
68 T. Agranov and B. Meerson, *Phys. Rev. Lett.*, 2018, **120**, 120601.
69 J. Liu, X. He, J. Z. H. Zhang and L.-W. Qi, *Chem. Sci.*, 2018, **9**, 2065–2073.
70 J. Guo, J. Lee, C. I. Contescu, N. C. Gallego, S. T. Pantelides, S. J. Pennycook, B. A. Moyer and M. F. Chisholm, *Nat. Commun.*, 2014, **5**, 5389.
71 M. F. A. Goosen, S. S. Sablani, H. Al-Hinai, S. Al-Obeidani, R. Al-Belushi and D. Jackson, *Sep. Sci. Technol.*, 2005, **39**, 2261–2297.
72 J. R. Werber, C. O. Osuji and M. Elimelech, *Nat. Rev. Mater.*, 2016, **1**, 16018.